



Inertial effects in just-saturated axisymmetric column collapses

William Webb¹ · Charles Heron¹ · Barbara Turnbull¹

Received: 4 May 2022 / Accepted: 1 April 2023
© The Author(s) 2023

Abstract

This work introduces a scaling analysis of sub-aerial axisymmetric column collapses of glass beads and Newtonian glycerol-water solutions mimicking some of the behaviours of debris flows. The beads were in a size range where their inertia partly decouples their collapse behaviour from the water column. Experiments explored a range of viscous, surface tension and particle inertia effects through systematic variation of particle size and fluid viscosity. Crucially a geotechnical centrifuge was used to access elevated effective gravitational accelerations driving the collapse, allowing field-scale viscous and surface tension effects to be replicated. Temporal pore pressure and run out front position evolution data was extracted using a pressure transducer and high speed imaging, respectively. A least-squares fitted scale analysis demonstrated that all characteristic dimensionless quantities of the acceleration phase could be described as a function of the column-scale Bond number Bo , the Capillary number Ca , the system size r^* , and the grain-fluid density ratio ρ^* . This analysis demonstrated that collapses as characterised by pore pressure evolution and front positions were controlled by the ratio of Bo/Ca . This indicates that grain-scale surface tension effects are negligible in such inertial column collapses where they may dominate laboratory-scale granular-fluid flow behaviour where geometric similarity between grain and system size is preserved.

Keywords Granular collapse · Inertial regime · Just-saturated · Scaling analysis · Centrifuge modelling

1 Introduction

Debris flows are a subset of gravity-driven slope hazards comprising a mixture of grains (rocks, soils) and water. The high fluid volume fraction and elevated relative density of the grains results in the forces developed in both phases significantly contributing to the dynamics of the mass movement [1]. The granular phase may also comprise a wide range of particle sizes [2], leading to complexity at both the grain- and macro-flow scales. With debris flows representing a significant geophysical hazard across the world [3], gaining an understanding of the roles of these different components

in controlling outcomes may help to effectively model and mitigate their destructive potential.

Information from naturally occurring debris flows is typically limited by the fact that initial and boundary conditions of the mass movement are generally unknown and material parameters obtained from the final flow morphology are poorly constrained [4]. In contrast, laboratory experiments offer a way to control all characteristics of the flow and contacting boundaries for the duration of the mass movement. Hence, data resulting from laboratory-scale flow experiments is repeatable and can be used to understand the influence of individual parameters on the flow's behaviour.

One experimental configuration that has received significant attention, because it replicates the unsteady nature of many geophysical flows, is the collapse of a granular step [5]. Generally performed on a granular column with an axisymmetric [5, 6] or quasi-two-dimensional [7] geometry, the column is suddenly released from its initial configuration and collapses until it reaches a stationary final deposit. While dry [5–8], fully-submerged [9] and wetted [10] granular material have all been used, fewer studies have investigated a situation more reminiscent of debris flows where the

Charles Heron and Barbara Turnbull authors contributed equally to this work.

✉ William Webb
evyww@nottingham.ac.uk
Charles Heron
Charles.Heron@nottingham.ac.uk
Barbara Turnbull
barbara.turnbull@nottingham.ac.uk

¹ Department of Civil Engineering, University of Nottingham, Nottingham NG7 2RD, UK

column is filled with fluid to a comparable depth to that of the granular material, which we term fully saturated.

The high travel speeds of full scale debris flows mean that even small particles exhibit inertial behaviour where the interaction between grain and fluid can be complex [2]. Dimensional analysis of a simple granular-fluid system suggests that the effects of surface tension are small compared to gravitational forces and fluid viscosity at the macro-scale of geophysical flows [11]. However, it has been found that the flow regime of a collapsing fluid-saturated granular column is primarily determined by the degree of capillary effects between the granular phase and the interstitial fluid due to surface tension [12].

However, as implied by the laboratory experiments, surface tension undoubtedly contributes to granular-scale flow mechanics, particularly at the flow's surface, and it remains possible that these processes can control mechanisms such as the build-up and dissipation of pore fluid pressure through capillary forces affecting macro-scale flow outcomes [13]. Several studies [e.g. 14, 15] have shown that the inclusion of high concentrations of fine granular material, like clays and silts, enhance the development of excess pore pressures which reduces the frictional resistance exerted on the bulk flow by the terrain bed. Coupled with the small number of physical studies investigating this phenomenon, the fact that recent numerical models [e.g. 16, 17, 18] have not reached a consensus on the most appropriate way to tractably model the mechanisms driving spatio-temporal variations in the grain size distribution suggests that we do not comprehensively understand the mechanisms at play or how their influence scales. Given the comparative micro-scale over which the interactions between the granular fines and the interstitial fluid occur, provided that a sufficient concentration of granular fines is present in the flow, it seems reasonable to suggest that surface tension may play a role in the development of these excess pore pressures and, hence, influence the macro-scale behaviour of the flow.

One way to try and replicate the stress-dependent processes present in natural scale flows within a laboratory model is to utilise a physical modelling method commonly used in the field of Geotechnical Engineering called Centrifuge modelling. By spinning a laboratory-scale model on an arm, the centripetal acceleration from the rotation becomes an effective gravitational acceleration. Thus, the effects of gravity on large 'prototype' structures can be replicated at a small physical scale through enhancing the effective gravitational acceleration [19]. The laboratory model is submitted to the required gravitational acceleration in order to replicate the stress profile within the modelled prototype scenario. The stress-similarity is achieved by attaching the model to the end of a centrifuge beam and submitting it to an elevated gravitational acceleration G which is N times larger than Earth's gravity g [20].

In the past two decades, there have been a number of significant works where centrifuge modelling has been used to physically investigate the scaling of the kinematic processes driving granular flows [e.g. 21, 22, 23]. More recently, the focus has shifted to the design of granular flow mitigation structures and the impact forces developed by the flow-structure collision [e.g. 24, 25]. However, the added complexity of a fluid phase has meant that the use of centrifuge modelling to study debris flows, to date, has been quite limited mainly focusing on debris flow initiation [20] and propagation [26].

The current study aims to provide a platform to investigate the role of micro-scale surface tension effects on macro-scale debris flow behaviour by first characterising the collapse response of grain-fluid mixtures with inertial grains by performing axisymmetric fluid-saturated granular column collapse tests using a geotechnical centrifuge. The use of the centrifuge allows a parameter space of particle size, surface tension and fluid viscosity to be explored in regimes where the grains are inertial and surface tension effects should have little influence on macro-scale flow outcomes.

2 Dimensional analysis

The initial geometry of an axisymmetric, fluid saturated, granular column collapse (see Fig. 1), can be described by two parameters; the initial height of the shared free-surface of the granular-fluid mixture h_0 , and the radius of the column prior to collapse initiation r_0 . Assuming that the granular phase is comprised of identical spherical particles situated in a homogeneous packing, the granular phase of the column can be characterised by the particle diameter d , the particle density ρ_p and the mean solid volume fraction of the column ϕ_p . Similarly, a Newtonian fluid phase can be characterised by the fluid density ρ_f , the fluid dynamic viscosity μ_f , and the fluid surface tension σ_f . While the initial system is fully

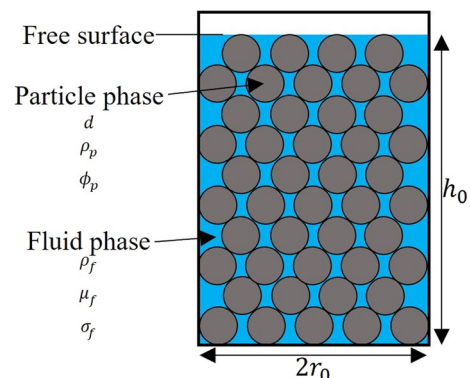


Fig. 1 Schematic of the initial configuration of a just saturated granular column collapse

saturated, as the collapse progresses, it is possible to obtain flow regions where the depth of the fluid phase is different to that of the granular phase. This can lead to the degree of saturation, the porosity of the granular media, and the surface tension of the fluid phase to significantly influence collapse dynamics.

The current analysis is interested in analysing the evolution of the phase front velocities u_x , where subscript x can refer to the fluid f or particle p phases, and the basal fluid pressure gradient at the centre of the column \dot{P} with time t throughout the duration of the column collapse. A promising place to start to understand this complex system is by utilising Buckingham’s Π theorem [27] to systematically identify dimensionless variables, termed Π groups, that provide a homogeneous solution to the physical relationships between key geometric and material parameters, and measured test data. Assuming a constant of gravitational acceleration $G = Ng$, where N is a constant and g is Earth’s constant of gravitational acceleration, it is hypothesised that a relationship between u_x and the other defined variables can be postulated as

$$u_x = f_1(h_0, r_0, d, \rho_p, \phi_p, \rho_f, \mu_f, \sigma_f, \dot{P}, t, G) \tag{1}$$

where f_1 is an unknown function. The primary difference between Eq. 1 and other relationships used in previous analyses to describe simplified debris flow motion [e.g. 1, 11], is the inclusion of fluid surface tension as a parameter. In contrast to previous analyses, we include fluid surface tension here as a controlling parameter to understand how, in a regime where particle inertia can dilate the granular phase, micro-scale interactions in the pore space may influence macro-scale outcomes.

Temporarily excluding ϕ_p as it is a dimensionless quantity, the other 11 variables within Eq. 1 are derived from combinations of three fundamental physical dimensions: mass, length and time. Hence, Buckingham’s Π theorem dictates that the variables can be connected by $11 - 3 = 8$ independent dimensionless Π groups. Following a previously described mathematical process [11], Eq. 1 can be rewritten as

$$\frac{u_x}{\sqrt{GL}} = f_2 \left(\frac{h_0}{r_0}, \frac{r_0}{d}, \frac{(\rho_p - \rho_f)N}{\rho_f}, \frac{t}{\sqrt{L/G}}, \frac{\dot{P}}{\rho_f \sqrt{G^3 h_0}}, \frac{\rho G h_0 d}{\sigma_f}, \frac{\mu_f \sqrt{G h_0^3}}{\sigma_f d}, \phi_p \right) \tag{2}$$

where f_2 is an unknown function, L is a characteristic length scale and ρ is the effective density of the granular-fluid column calculated as $\rho = \phi_p \rho_p + (1 - \phi_p) \rho_f$. The characteristic length scale L has been intentionally left arbitrary allowing

us to explore this dimensionless space over both the column and grain scales (see Sect. 6).

The left-hand side of Eq. 2 takes the form of a phase Froude number Fr_x where again, the subscript x refers to the phase of interest. Fr_x compares the influence of inertial and gravitational forces at the phase flow front over the length scale of interest. The right-hand side is comprised of eight dimensionless groups that are used to determine Fr_x . The first parameter is the column aspect ratio a which has been shown to be the dominant parameter in the scale analysis of dry granular column collapses. The second parameter was defined as the system size [8] r^* and was shown to have some influence on the evolution of the dry collapse case. The third parameter is the relative granular-fluid density ratio accounting for acceleration-scale buoyancy ρ^* . When $N = 1$, ρ^* reduces to the simple mass ratio found in traditional fluid-granular flow scale analyses [e.g. 1]. Whereas, when $N > 1$, the enhanced gravitational field acts on the difference in densities, normalised as a reference density, as a buoyancy. The fourth parameter, t^* , is the ratio between t and a characteristic inertial timescale $\sqrt{L/G}$ where, again, L refers to the characteristic length scale of interest. The fifth parameter, \dot{P}^* , is the ratio between \dot{P} and the equivalent hydrostatic pressure gradient down the initial height of the column. The sixth parameter is the column Bond number Bo and is defined as the ratio between the inertial forces at the column scale that drive the collapse of the column and the capillary forces at the grain scale induced by deformation of the fluid-air interface. Its influence over the collapse regime of a fluid-saturated granular material under Earth’s gravitational acceleration has already been highlighted [12]. The seventh parameter is known as the Capillary number Ca and relates the viscous forces within the fluid at the column scale to surface tension effects at the grain scale. The final parameter is ϕ_p which remains unchanged since it is already dimensionless. The inclusion of both Bo and Ca as Π groups of interest is crucial for ensuring that macro-scale inertial and viscous forces are scaled appropriately in relation to grain-scale surface tension effects in order to obtain a granular phase whose behaviour is primarily governed by particle inertia. Here, we use centrifuge modelling to extend the accessible model parameter space for a simple axisymmetric, fluid-saturated, column collapse configuration. Hence, we are able to perform a multi-scale analysis of the problem by varying G rather than adapting the physical size of the experimental configuration.

It is important to note that the solution to Eq. 2 is not unique. The resulting Π groups could have been recast into alternative forms. In particular, Ca could be replaced by other previously studied dimensionless quantities like the Stokes St (characteristic particle timescale against characteristic fluid timescale) or Reynolds Re (inertial forces against viscous forces in the fluid) numbers. Ca was determined as

the most useful parameter out of this group given that the influence of surface tension has been shown to vary with scale [11].

Crucially, four of the dimensionless groups within Eq. 2 contain N or G suggesting that the behaviour of the analysed system is highly scale dependent. Hence, to sufficiently determine the contributions of these dimensionless groups to collapse behaviour, a multi-scale analysis would be required. Given that the size of an experimental configuration is often limited in a laboratory setting, this type of analysis is unworkable with most laboratory-scale granular-flow test configurations.

3 Model apparatus

Experiments were conducted using the University of Nottingham's GT50/1.7 geotechnical beam centrifuge. The centrifuge has a platform radius of 2 m and is attached to a swinging platform capable of supporting a payload up to 0.9 m high, 0.6 m circumferential and 0.8 m wide [30]. The machine is capable of applying a maximum centripetal acceleration of 150 g to a payload up to 335 kg in mass.

Within a wind-proof strong box, a steel cylinder with an inner radius $r_0 = 54$ mm was positioned in the centre of a 490 mm by 485 mm flat plexiglass sheet (see Fig. 2). A foam o-ring was fixed to the base of the steel cylinder allowing a seal to form between the cylinder and the plexiglass when downward pressure was applied to the cylinder. The cylinder was held in a fixed position by two steel rods that were screwed into the top of the column and tightly pressed against a forked steel plate.

Throughout testing, the cylinder was filled to an initial height $h_0 = 50$ mm of both grains and fluid, creating a just-saturated column with $a = 0.93$. Several previous studies have investigated the effects of varying a in both the axisymmetric [5, 6, 8] and quasi-two-dimensional [7, 31] collapse. So here, we focus on column configurations where $a \approx 1$,

matching a number of reviewed geophysical collapse events [32]. A 12 V LED lightsheet was installed beneath the plexiglass sheet, which acted as a diffuser, creating even back-lighting of the test surface.

The fluid-saturated granular column was comprised of spherical soda lime glass beads and an interstitial fluid consisting of a miscible glycerol-water mixture. Table 1 details the range of values used for all test parameters of interest. The tested centrifuge rotational speeds were selected such that the tested values of N relative to the centrifuge cradle were 1, 5, 15 and 30. These values were then adjusted so that they were relative to a height of $\frac{2}{3}h_0$ above the horizontal plane to account for variations in centrifugal acceleration across the height of the column. Higher rotational speeds were not explored as the resolution of the recorded videos were limited by the frame rates of the cameras.

Table 2 provides a summary of the parameter space obtained across testing for the dimensionless groups from Eq. 2 calculable from the geometric and material property information given in Table 1. Given that the Bond number is always significantly larger than unity while the tested Capillary numbers cover a range of magnitudes smaller and larger than unity, it is evident that the parameter space explored by the current experiments includes flow states that are largely dominated by gravitational forces at the column-scale while the relative influence of surface tension at the grain-scale and viscous forces at the column-scale vary depending on the geometry of the initial column and test material properties.

It should be noted that previous studies [8, 33] have concluded that axisymmetric column collapse experiments conducted over the specified range of r^* are highly susceptible to grain-size effects which can significantly influence the mobility and duration of the collapses. However, by not adhering to the geometric reality of the natural scale, we are able to ensure that the behaviour of the spherical particles is primarily governed by their inertia. As such, the current study complements previous work by focusing on a collapse

Fig. 2 Schematic of experimental setup

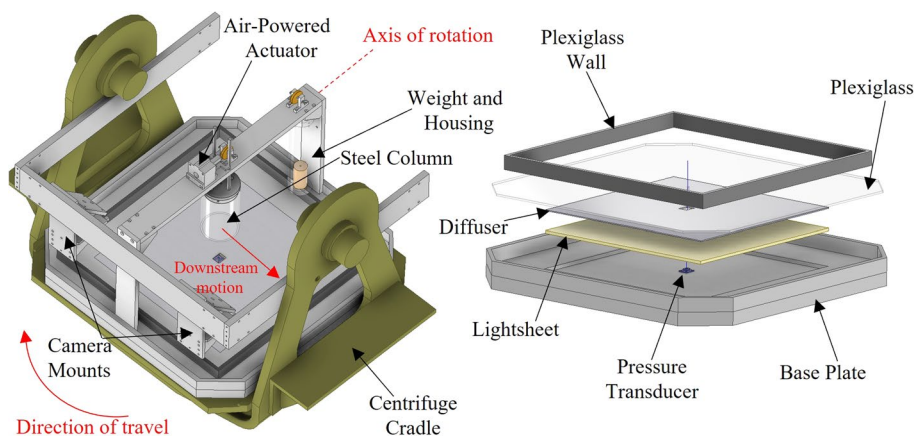


Table 1 Summary of experimental test parameters

Experimental parameters	Symbol	Definition	Range
Initial column height	h_0		50 mm
Initial column radius	r_0		54 mm
Centrifuge rotational speed	R		[0, 47, 82, 116] rpm
Gravitational scale factor ^a	N		[1, 4.6, 14, 28.1]
Temperature of fluid phase	T		20 ± 2 °C
Particle diameter	d		[2, 4, 6, 8] mm
Particle density	ρ_p		2642 ± 27.4 kg m ⁻³
Mean solid volume fraction ^b	ϕ_p	$M_p / (\pi r_0^2 h_0 \rho_p)$	0.61 ± 0.01
Glycerol mass concentration	C_m	$M_g / (M_g + M_w)$	[0, 0.1, 0.52, 0.69, 0.77]
Water density ^b	ρ_w		1000 kg m ⁻³
Glycerol density ^c	ρ_g		1260 kg m ⁻³
Fluid mixture density	ρ_f	$C_m \rho_g + (1 - C_m) \rho_w$	1000 - 1201 kg m ⁻³
Fluid mixture viscosity ^d	μ_f	$\mu_0 \left[\frac{1 - C_m/C}{1 - (k_0 C - 1) C_m/C} \right]^{(-2.5C)/(2 - k_0 C)}$	1 - 52.1 cP
Water surface tension ^c	σ_w		72.5 mN m ⁻¹
Glycerol surface tension ^c	σ_g		63.4 mN m ⁻¹
Fluid mixture surface tension	σ_f	$C_m \sigma_g + (1 - C_m) \sigma_w$	65.5 - 72.5 mN m ⁻¹

^a Calculated using an effective radius of 1.87 m between the centrifuge’s axis of rotation and $\frac{2}{3}h_0$ from the base of the column to account for variations in centrifugal acceleration across the height of the column

^b Formula used by Warnett et al. [8]

^c Obtained from Lide [28] for a temperature of 20 °C

^d Eq. 11 from Takamura et al. [29] where $\mu_0 = 1$ cP (i.e. the viscosity of water at 20 °C), constant $C = 1.2$ and $k_0 = -0.012(T + 273.15) + 4.74$

Table 2 Summary of the dimensionless parameter space calculable from the geometric and material property information in Table 1

Dimensionless variables	Range
a	0.93
r^*	6.75 - 27.0
ρ^*	1.63 - 35.0
Bo	26.6 - 3480
Ca	0.06 - 45.2

regime where the influence of particle inertia is promoted instead of grain scale.

3.1 Test procedure

The fully-saturated granular column was prepared after the model was loaded onto the centrifuge. A predefined mass of granular material M_p was poured into the tube which had been previously filled by a predefined volume of interstitial fluid V_f where the respective mass of water M_w and glycerol M_g used was defined by the glycerol mass concentration required for that test. The column was compacted from the top using a steel rod until the desired initial column height $h_0 = 50$ mm was achieved, and the surface of the fluid was level with the top of the grains. The repeatability of this preparation method is demonstrated by the small range of

ϕ_p values achieved across all tests as stated in Table 2. While the achieved packing fractions suggest that the column packing configuration can be described as a poured random packing [34], we follow the logic of previous authors [e.g. 13, 17] by assuming that the granular column is initially in a dense configuration as ϕ_p is greater than the critical solid volume fraction $\phi_c = 0.6$ which is generally used as a criteria to assess whether a granular flow is going to contract or dilate.

Prior to initiating collapse, the centrifuge with the experiment mounted on it was spun up to a speed submitting the model to an enhanced gravitational acceleration $G = Ng$ where $g = 9.81$ m s⁻². Once spun up, a weighted pulley system was triggered by an air-powered actuator to lift the cylinder and initiate the collapse of the fully-saturated granular column over the horizontal test plane. From analysis of the raw basal pressure data and the high-speed camera footage, the time scale for the cylinder to be lifted up to a height of h_0, t_{col} , can be approximately calculated as $t_{col} \approx 2.5 \sqrt{h_0 / (Ng)}$. This equates to a mean release velocity that obeys Sarlin et al.’s [35] criterion for a release process that has no influence on the dynamics of a quasi-two-dimensional collapse consisting of dry spherical glass beads. Li et al. [36] suggested that a lower release velocity may be satisfactory to achieve this effect for wetted granular material given the potential build-up of cohesive forces between adjacent grains. Further investigation is required to confirm

this theory and extend it to the fully saturated regime, as well as considering other collapse geometries like the axisymmetric case. However, we deem the dry criterion to be sufficient for the current study.

3.2 Front measurement

Lifting the steel cylinder initiated the collapse of the fluid-saturated granular column. The temporal evolution of the collapse was recorded by two Go-Pro cameras at a resolution of 1080×1920 pixels and an acquisition rate of 240 frames per second. The images were first treated for fisheye distortion effects [37]. The experimental spatial domain within the images is then calibrated using black markers positioned around the edge of the lightsheet. The markers are used within the digital image correlation (DIC) scheme developed by Blaber et al. [38] to produce an orthonormal image plane. Radial distance values could be taken from the post-processed images at a spatial resolution of 0.5 mm. The upstream and downstream directions, which refers to whether the flow is propagating with (upstream) or against (downstream) the relative motion of the centrifuge, of the collapse are recorded on separate cameras to improve image resolution. This also allows for the contributions of Coriolis acceleration and the Eötvös effect to be considered [19] with respect to the upstream and downstream directions of motion as shown in Fig. 2.

Figure 3 shows the collapse evolution of two test cases, both with $d = 8$ mm, at $N = 1$ [(a)–(e)] and $N = 14$ [(f)–(j)] from the downstream direction. A multi-threshold image analysis scheme was developed to create masks of the individual fluid and particle phases for each image frame. These calibrated masks were then used to obtain the averaged

instantaneous front positions, $r_{f,i}$ and $r_{g,i}$, and the final front positions, $r_{f,F}$ and $r_{g,F}$, of the fluid and particle phases, respectively. Tracking the phase fronts separately was necessary in order to evaluate how variations in the chosen parameter space affected phase front interactions.

For tests that remained within the measurement domain [(a)–(e)], $r_{f,F}$ and $r_{g,F}$ are defined as the position of the phase fronts when the collapsing material ceases to move which is formalised as an average fluid front velocity less than $2.4 \times 10^{-3} \text{ m s}^{-1}$ (0.01 mm per frame). However, for tests at elevated G , $N > 1$, [(f)–(j)] the propagation of the two phases extended beyond the measurement area. In these cases, $r_{f,i}$ and $r_{g,i}$ were taken as the average radial distance of the respective phase fronts from the final image frame, where the entirety of both phase fronts remained inside the measurement area.

3.3 Pore pressure measurement

The evolution of basal fluid pressure under the centre of the granular column was measured with a miniature pressure transducer (PT) which was covered by a sheet of filter paper. The sensor had a pressure range of 200 kPa and recorded data at a frequency of 125 kHz. Measurement accuracy was found to be ± 0.1 kPa by calculating the average reading error when supplying a known pressure to the transducer. Figure 4 provides an example of the filtering strategies implemented to clean the signal for a collapse test where $d = 2$ mm, $N = 4.6$ and $C_m = 0$. From the data, a number of different effects can be seen. In particular, the large spike in pressure located around 0.16 – 0.17 s after collapse initiation is a result of the vibrations across the run out surface emanating from the weight used to lift the steel column

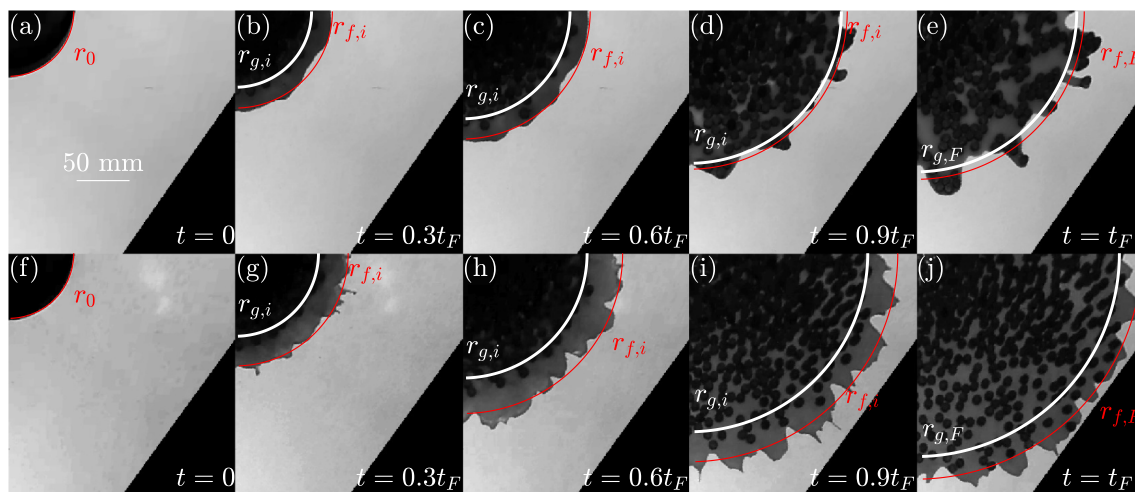


Fig. 3 Snapshots of the collapse sequence downstream of centrifuge motion for two columns, both with $d = 8$ mm, with gravitational acceleration coefficient $N = 1$ [(a)–(e)] and $N = 14$ [(f)–(j)]. The

averaged radial position of the fluid (red) and particle (white) phase fronts, where the top left of each image is the point of origin, are shown (colour figure online)

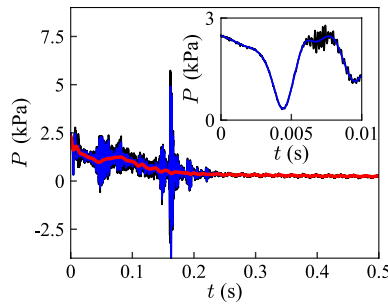


Fig. 4 Time evolution of basal fluid pressure at the centre of the column, P , for $d = 2$ mm, $N = 4.61$ and $C_m = 0$. The column collapse was initiated at time $t = 0$. The raw signal (black), the reconstructed signals filtered with $f_c = 1000$ Hz (blue), and $f_c = 100$ Hz (red) are all shown. The inset shows the magnified initial pressure evolution of the test demonstrating how well the reconstructed signal with $f_c = 1000$ Hz captures the early pressure drop and recovery (colour figure online)

colliding with the actuator located at the bottom of its housing. Given that signal noise comprised a number of identifiable elements such as this vibration, Fourier transformations of the signal were used to define a cutoff frequency f_c for a low-pass filtering scheme.

The overall trend of the signal, highlighted in red in Fig. 4, from collapse initiation through to run out completion, was approximated using a fourth-order low-pass digital Butterworth filter with $f_c = 100$ Hz within the Matlab [39] signal processing toolbox. Pressure changes relating to column dilation occurring over the first few milliseconds of the collapse were also of interest and were captured using a higher cutoff frequency equal to $f_c = 1000$ Hz. The inset of Fig. 4 demonstrates the filtering schemes ability to capture the significant pressure drop and recovery at the onset of collapse. Pore pressure measurements were only considered for tests where $N > 1$ to ensure that the noise of the signal was less significant than the total drop in pressure. Pressure measurements were also not recorded for tests undertaken at $N = 28.1$.

4 Column mobility

The influence of particle size d and gravitational acceleration N on the temporal evolution of the collapse front was investigated by examining the temporal evolution of $r_{f,i}$ from time $t = 0$ until the time where $r_{f,F}$ is achieved t_F . Figure 5 presents the evolution of the difference between the instantaneous fluid phase front position and the initial fluid phase front position normalised by the initial fluid phase front position, known as the normalised fluid run out length, $(r_{f,i} - r_{f,0})/r_{f,0}$ for particle diameters $d = 2$ mm, $d = 4$ mm, $d = 6$ mm, and $d = 8$ mm, at $N = 1$, $N = 4.61$ and

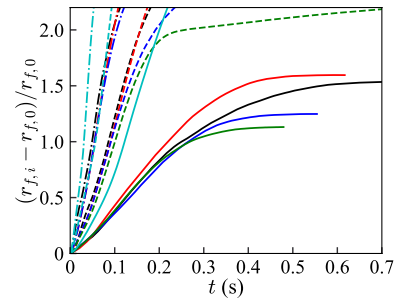


Fig. 5 Temporal evolution of the normalised fluid run out length $(r_{f,i} - r_{f,0})/r_{f,0}$ in time t for particle sizes $d = 2$ mm (green), $d = 4$ mm (blue), $d = 6$ mm (red), $d = 8$ mm (black) at $N = 1$ (line), $N = 4.6$ (dashed) and $N = 14$ (dot-dashed) downstream of centrifuge motion. Collapses of a grain-free fluid phase (cyan) at all values of N are also shown (colour figure online)

$N = 14$, downstream of centrifuge motion. Figure 5 also includes data from a set of experiments where the column had no grains, just the fluid phase, illustrating the limiting case (i.e. $d = 0$ mm) for each N . The selected tests have a constant μ_f at each value of N with $\mu_f/\mu_w = [1, 6.7, 21.5]$ for $N = 1$, $N = 4.61$ and $N = 14$.

Tests at $N = 1$ appear to follow the three distinct collapse stages described by previous authors [5, 6, 8]. On initiation, the flow front initially accelerates to reach a state of quasi-steady flow. In the run out phase, the flow retards until movement ceases and the final deposit is formed where $r = r_{f,F}$. The time at which $r = r_{f,F}$, $t_{f,F}$, for these test cases increases with grain size d , similar to the relationship found by Bougouin et al. [12]. That study reasoned that the capillary forces between grains, whose magnitude is controlled by the level of surface tension between the interstitial fluid and the ambient air, was the key contributor to this phenomena. Larger capillary forces are present within granular mixtures with smaller pore spaces, an allegory of particle size, which restricts the mobility of grains and results in a lower $t_{f,F}$ value. Even though the particle sizes used in the current study are at the top end of the particle sizes used by Bougouin et al., suggesting that the current regime is primarily controlled by inertial forces, the influence of surface tension is still identifiable in this run out stage. This may result from a number of factors including; fluid seepage scaling more strongly with N than grain scale inertia [40, 41], the high free surface energy of plexiglass which increases its wettability and aids the propagation of a fluid film across its surface [42] and, particle clustering that can lead to localised capillary effects which reduces the speed of the granular phase.

In contrast, for $N > 1$, $t_{f,F}$ primarily decreases with increasing pore space. This trend tends towards the edge case of the collapse of the singular fluid phase. Similarly to the case of $N = 1$, the retardation present in the

temporal evolution of the tests containing a granular phase is due to surface tension giving rise to capillary forces which reduces flow mobility. Crucially, by comparing to the edge case, it is evident that the level of retardation reduces with increasing N , suggesting that the influence of capillary forces on the temporal evolution of the collapse reduces with increased scale. This result is reassuring as the macro-scale behaviour of geophysical-scale debris flows are predominantly controlled by gravitational and viscous forces [11].

Given that the interaction between the granular and fluid phases has been shown to significantly affect flow mobility, it is logical to consider the temporal evolution of both constitutive phases through their relative positions to one another. Figure 6 shows the evolution of the normalised distance between the fluid and granular phase fronts $(r_{f,i} - r_{p,i})/r_{f,i}$ with normalised time t/t_F for particle diameters $d = 2$ mm, $d = 4$ mm, $d = 6$ mm, and $d = 8$ mm, at $N = 1$, $N = 4.61$, $N = 14$ and $N = 28.1$ for the upstream and downstream propagation directions. Similarly to Fig. 5, tests have been selected so all tests conducted at the same N use interstitial fluids with the same viscosity. $\mu_f/\mu_w = 44.8$ for the tests conducted at $N = 28.1$.

Initially, all collapses exhibited a drainage phase where the fluid front accelerates away from the granular material. For a given value of N , the maximum distance between the two phase fronts increases with pore space as the space for the fluid to exit the granular structure increases while the influence of capillary effects reduce. For a given value of d , the maximum relative distance increases with N until $N = 14$. Increasing N to 28.1 sees a reduction in the maximum relative distance possibly resulting from the reduced impact of solid–fluid interactions as the flow becomes dominated by inertia.

Figure 6 also shows how the granular front's ability to catch up to the fluid front varies with d and N . The two fronts were considered to be approximately aligned when the normalised relative distance was less than 0.05. For all tests conducted with $N = 1$, the granular front was able to completely catch up to the fluid front by the end of the run out phase. The granular front did not overtake the fluid fronts

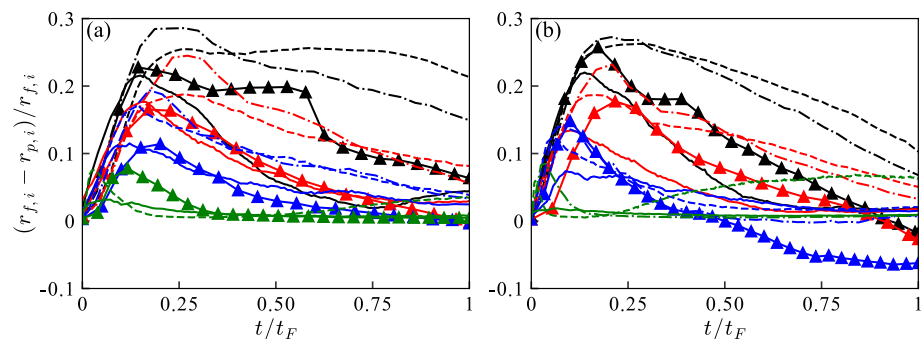
over the duration of these tests which is likely due to the significant impact that surface tension has on laboratory-scale granular–fluid flows.

For a given $d > 2$ mm and $N > 1$, the final separation between the two phase fronts reduced with increasing N . For collapses propagating in the downstream direction, the granular front was even able to overtake the fluid front for $N = 28.1$. It is clear that the enhanced gravitational acceleration field is supplying more kinetic energy to the granular phase which allows it to catch up to the fluid front. Hence, the separation between the two phase fronts reduces when a larger acceleration field (N) is applied.

Figure 6 also shows the influence of the Coriolis acceleration on the mobility of the flow. During the initial stages of the post-collapse propagation, the maximum separation between the two phase fronts for each test was generally greater for the collapsing section propagating in the downstream direction. This was somewhat expected as the Coriolis acceleration will promote the drainage and subsequent propagation of the fluid away from the centre of the test area in the downstream direction while impeding it in the upstream direction. Similarly, during the latter stages of recorded motion, the ability of the granular front to catch up to the fluid front, resulting in a lower final separation, also increased when aided by the Coriolis acceleration. Similar effects have been noted in recent numerical works [43, 44] where the density of the flow is highly dependent on the flow propagation direction relative to centrifuge motion. Naturally, the magnitude of these effects increased with N , as the magnitude of the Coriolis acceleration also increases with N .

While the influence of the Coriolis acceleration does vary with particle size, it only appears to have a significant affect on flow dynamics when the collapses containing smaller particle sizes (i.e. $d = 2$ mm) enter a 'creep-like' flow regime where, in the downstream direction, the fluid front is again able to accelerate away from the granular front. Whereas, for the larger particle sizes, the Coriolis force only further propagates the reduction of $(r_{f,i} - r_{p,i})/r_{f,i}$ with normalised time. Similarly, the influence of the Eötvös effect appeared to be negligible on flow dynamics prior to the creep phase which is likely due to the fact that natural scale particle inertia

Fig. 6 Temporal evolution of the normalised distance between the phase fronts $(r_{f,i} - r_{p,i})/r_{f,i}$ against normalised time t/t_F for particle sizes $d = 2$ mm (green), $d = 4$ mm (blue), $d = 6$ mm (red), $d = 8$ mm (black) at $N = 1$ (line), $N = 4.6$ (dashed), $N = 14$ (dot-dashed) and $N = 28.1$ (triangles) upstream (a) and downstream (b) of centrifuge motion (colour figure online)



has been preserved. Given that the current study focuses on debris flow mechanics, which are best replicated within the experiment prior to the flow entering a monolayer (i.e. the initial acceleration phase), we have deemed the asymmetry induced by the Coriolis acceleration and the Eötvös effect to be negligible for the particular collapse period of interest (see Sect. 6).

5 Fluid pressure evolution

As well as having a dominant effect on the possible separation between the two phase fronts, the drainage phase of the collapse is key to the dissipation of pore pressure from the initially static column configuration. Figure 7 details the evolution of the normalised basal fluid pressure at the centre of the column P with time t for particle diameters, $d = 2$ mm, $d = 4$ mm, $d = 6$ mm, and $d = 8$ mm, at (a) $N = 4.61$, and (b) $N = 14$, respectively. Again, tests have been selected that have a shared μ_f value for every value of N . In this case, the time-frame shown has been restricted to the first 0.5 s of each collapse at which point the residual normalised pressure is referred to as P_F^* .

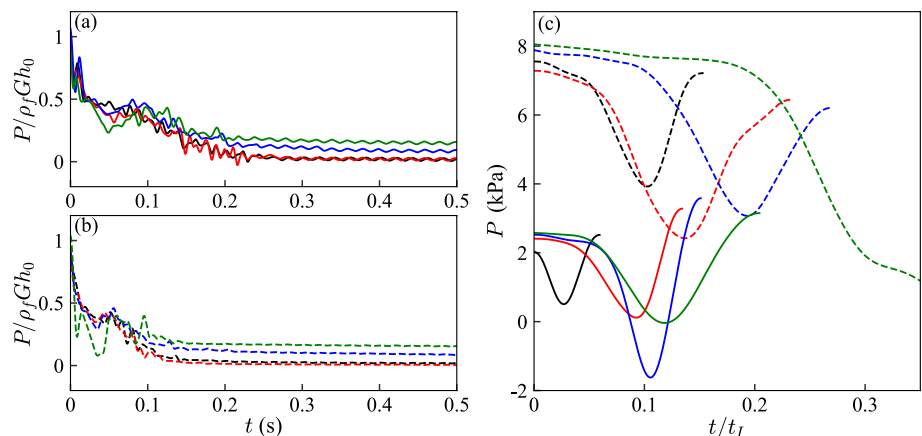
At the beginning of each test conducted at both $N = 4.61$ and $N = 14$, $P \approx \rho_f G h_0$ which illustrates that pressures within the column are hydrostatic prior to the collapse. Upon release, the height of fluid above the pressure sensor reduces throughout the collapse as the granular-fluid mixture propagates out away from the column centre. This results in a progressive reduction of P until $P = P_F^*$.

The influence of d on the temporal evolution of P can be illustrated through its influence of P_F^* . For a given N , P_F^* increases with decreasing d and P_F^* for particle sizes $d = 6$ mm and $d = 8$ mm is approximately equal to 0 kPa where no fluid remains above the PT. This demonstrates the reduced influence of the granular phase on P_F^* as d increases. It can be reasoned that the increased pore space improves the fluid’s ability to displace from the centre

of the measurement domain over the test duration. Conversely, a smaller pore space limits the fluid’s ability to exit the granular material which itself has reduced mobility due to capillary effects. A similar particle size dependency has been observed in the case of post-depositional seepage in natural scale debris flows [e.g. 45]. The influence of d also appears to slightly increase with N .

Figure 7c focuses on another characteristic feature of the evolution of P , which is the reduction and recovery of basal pore pressure observed over the inertial column timescale $t_I = \sqrt{h_0/G}$ immediately after collapse initiation. While the magnitude of this initial pressure reduction increases with N , the more interesting variation is largely controlled by d with the magnitude of the pressure drop generally increasing as d decreases for a given N . This effect is more pronounced when $N = 14$. The recovery of this initial pressure reduction also appears to reduce as N increases. As this variation in pressure reduction occurs immediately after the release of the column, it is likely to be the result of initial particle rearrangement. It has been found previously that the critical solid volume fraction for spherical grains $\phi_{p,c} \approx 0.57$ [13]. This suggests that all tests in the current study were conducted with dense granular packings which means that, upon the onset of the collapse, the granular structure must initiate its displacement by first dilating. This allows the interstitial pore fluid to move into the additional pore space created by the dilation which, based on the pore pressure feedback loop described by Iverson et al. [46], causes a reduction in basal fluid pressure. Rondon et al. [13] demonstrated the presence of the pore pressure feedback loop for a quasi-two-dimensional fully-submerged granular column collapse configuration exposed to the acceleration field of Earth’s gravity. The study was carried out using only a singular particle size ten times smaller than the smallest particle used in the current work. A submerged collapse would not experience any influence from surface tension so any differences in behaviour based on particle size would

Fig. 7 Temporal evolution of the dimensionless basal fluid pressure at the centre of the column $P/\rho_f G h_0$, filtered using $f_c = 100$ Hz with time t for particle sizes $d = 2$ mm (green), $d = 4$ mm (blue), $d = 6$ mm (red), $d = 8$ mm (black) at (a) $N = 4.61$ (line) and (b) $N = 14$ (dashed). (c) Basal fluid pressure at the centre of the column P , filtered at $f_c = 1000$ Hz, against t/t_I immediately after the release of the column (coloured figure online)



emanate from viscous interactions between the fluid and the grains. In the current configuration, capillary forces arising from the presence of surface tension will cause a further reduction in P .

6 Scale analysis

As collapse dynamics clearly depend on N , dimensionless parameters used previously in the literature, a and ϕ_p , are not enough to characterise the phenomena governing the behaviour of the fluid-saturated granular column collapse in the current test configuration. The observed interplay between the fluid and particle fronts also suggests that the viscous nature of the interstitial fluid must also be recognised to explain these flow states.

To characterise the acceleration phase of each collapse, the maximum velocities of the two phase fronts $u_{f,m}$ and $u_{p,m}$, and the time after collapse initiation that these maximum velocities were achieved $t_{f,m}$ and $t_{p,m}$, were evaluated. A linear approximation of the pressure gradient over the first significant pressure drop at the centre of the column, \dot{P}_m , was recorded as indicative of the pore pressure response in the early collapse stages. Using these terms, Eq. 2 can be rewritten into the following form

$$\frac{u_{x,m}}{\sqrt{GL}} = f_3 \left(\frac{h_0}{r_0}, \frac{r_0}{d}, \frac{(\rho_p - \rho_f)N}{\rho_f}, \frac{t_{x,m}}{\sqrt{L/G}}, \frac{\dot{P}_m}{\rho_f \sqrt{G^3 h_0}}, \frac{\rho G h_0 d}{\sigma_f}, \frac{\mu_f \sqrt{G h_0^3}}{\sigma_f d} \right) \tag{3}$$

where f_3 is an unknown function and, again, the subscript x refers to the phase of interest. Noting that ϕ_p remained approximately constant throughout the experiments, this parameter was disregarded from all further analyses. Thus eight dimensionless groups are defined: $Fr_{x,L}$, a , r^* , ρ^* , $t_{x,L}^*$, \dot{P}_m^* , Bo and Ca , where subscript x , again, refers to the phase of interest and subscript L is equal to d or h_0 depending on the characteristic length scale of interest.

Values of $Fr_{x,L}$ and $t_{x,L}$ were obtained for each test by averaging the upstream and downstream values of V_x and t_x , respectively. This had the added benefit of limiting the contributions of Coriolis acceleration and the Eötvös effect on the scale analysis. The significance of each parameter in Eq. 3 was tested through the implementation of a non-linear regression scheme with a weighting that favoured power-law fits that minimised the degrees of freedom to reasonably portray the data set. Given that we do not have an a priori understanding of the combined and relative influence of each Π group within the dimensionless parameter space,

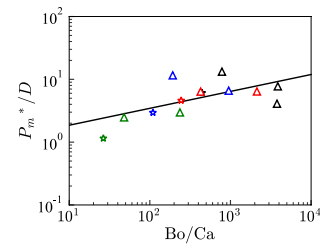


Fig. 8 \dot{P}_m^* normalised by $D = (\rho^*)^\beta (r^*)^\gamma$ against Bo / Ca for particle sizes $d = 2$ mm (green), $d = 4$ mm (blue), $d = 6$ mm (red), $d = 8$ mm (black) at $N = 4.61$ (triangle) and $N = 14$ (star). The black line indicates the power law fit provided in Eq. 4 using the exponents found in Table 3 (colour figure online)

Table 3 Summary of exponents used to fit Eq. 4 for all characteristic dimensionless quantities of interest. The normalised root mean squared error $RMSE_N$ of each fit is also detailed

Q	α	β	γ	$RMSE_N$
$Fr_{f,d}$	-0.04	0.07	0.30	0.15
Fr_{f,h_0}	-0.02	0.08	-0.25	0.27
$Fr_{p,d}$	-0.04	0.04	0.34	0.13
Fr_{p,h_0}	-0.04	0.04	-0.16	0.31
$t_{f,d}^*$	0.07	0.18	0.54	0.09
t_{f,h_0}^*	0.07	0.18	0.04	0.16
$t_{p,d}^*$	0.10	0.16	0.50	0.13
t_{p,h_0}^*	0.13	0.13	-0.03	0.17
\dot{P}_m^*	0.27	-0.46	0.80	0.26

a generalised power-law fit provides a reasonable starting point for this process. The outcome is that all measured quantities, meaning \dot{P}_m^* , $Fr_{x,L}$ and $t_{x,L}^*$, appear to be independent of each other for all phases and scales. Figs. 8, 9 and 10 show the finalised fits for \dot{P}_m^* , $Fr_{x,L}$ and $t_{x,L}^*$ against Bo / Ca , respectively. The low measurement error for the majority of points in Figs. 8 and 9 further highlights the minimal influence that the Coriolis acceleration had over the collapse period of interest. In the case of \dot{P}_m^* , the absolute measurement error for each data point lies within each respective marker. It is important to note that this error differs from the fluctuations in pressure gradient throughout the signal which is significantly larger. The variation of all measured quantities of interest Q can be described by the following relation

$$Q = \left(\frac{Bo}{Ca} \right)^\alpha (\rho^*)^\beta (r^*)^\gamma \tag{4}$$

where α , β and γ are constants that are summarised in Table 3. Equation 4 demonstrates that the selected characteristic quantities associated with the initial acceleration phases of the granular and fluid flow fronts and the initial

post-collapse pressure gradient can be reasonably well predicted by a simplistic power law model consisting of three dimensionless parameters.

6.1 Quantification of scaling parameter influence

Equation 4 provides significant insight into the factors governing the behaviour of these characteristic flow states. The relative influence of each parameter on the right-hand side

of Eq. 4 on the mobility of the granular and fluid phases is investigated further in Fig. 11 where each parameter to the power of its exponent is plotted against itself for all variations of $Fr_{x,L}$ and $t_{x,L}^*$.

Considering Bo/Ca as a single parameter within Eq. 4 means that the fits of Q are decoupled from the influence of surface tension at the grain-scale. Instead, it is the balance of column-scale gravitational and viscous forces that influence flow behaviour. While the influence of surface tension at

Fig. 9 $Fr_{x,L}$ normalised by $D = (\rho^*)^\beta (r^*)^\gamma$ against Bo/Ca for particle sizes $d = 2$ mm (green), $d = 4$ mm (blue), $d = 6$ mm (red), $d = 8$ mm (black) at $N = 1$ (cross), $N = 4.61$ (triangle), $N = 14$ (star) and $N = 28.1$ (circle). (a) $x = f$ and $L = d$, (b) $x = f$ and $L = h_0$, (c) $x = p$, and $L = d$ and (d) $x = p$ and $L = h_0$. The black line indicates the power law fit provided in Eq. 4 using the exponents found in Table 3. Error bars signify the absolute measurement error of the independent variable (colour figure online)

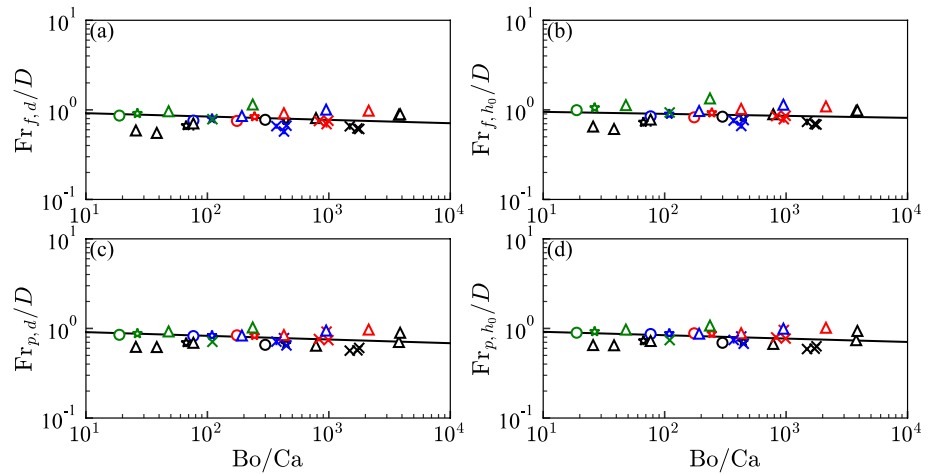


Fig. 10 $t_{x,L}^*$ normalised by $D = (\rho^*)^\beta (r^*)^\gamma$ against Bo/Ca for particle sizes $d = 2$ mm (green), $d = 4$ mm (blue), $d = 6$ mm (red), $d = 8$ mm (black) at $N = 1$ (cross), $N = 4.61$ (triangle), $N = 14$ (star) and $N = 28.1$ (circle). (a) $x = f$ and $L = d$, (b) $x = f$ and $L = h_0$, (c) $x = p$, and $L = d$ and (d) $x = p$ and $L = h_0$. The black line indicates the power law fit provided in Eq. 4 using the exponents found in Table 3. Error bars signify the absolute measurement error of the independent variable (colour figure online)

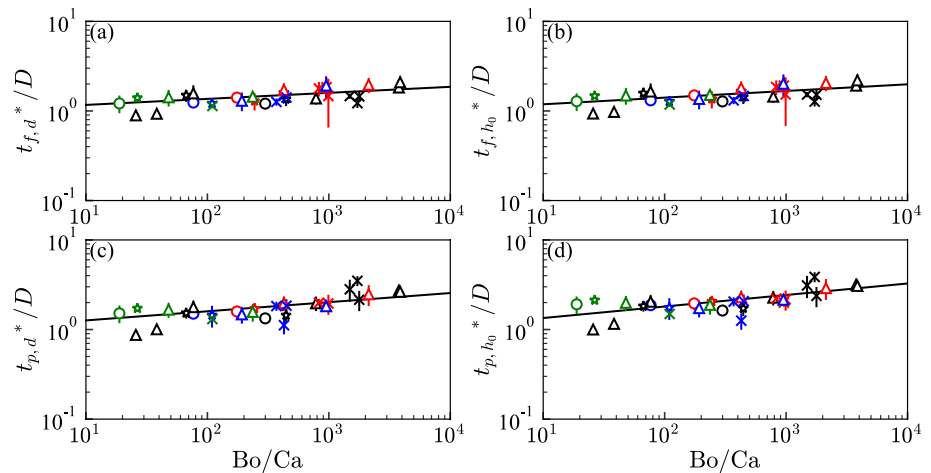
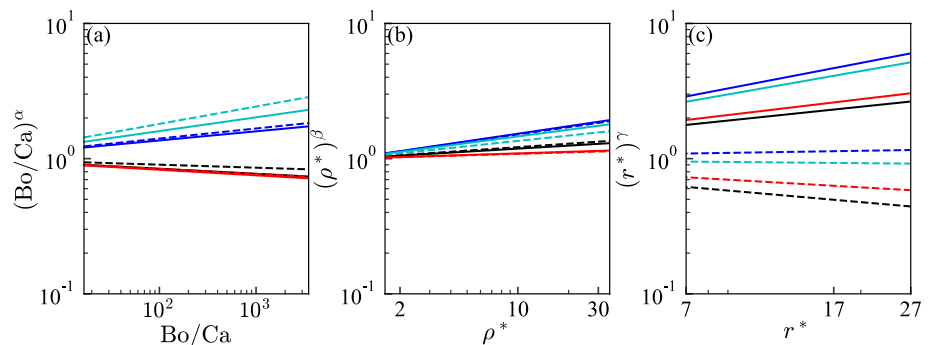


Fig. 11 (a) $(Bo/Ca)^\alpha$ against Bo/Ca . (b) $\rho^{*\beta}$ against ρ^* . (c) $r^{*\gamma}$ against r^* . Fits for $Fr_{f,d}$ (black), Fr_{f,h_0} (black dashed), $Fr_{p,d}$ (red), Fr_{p,h_0} (red dashed), $t_{f,d}^*$ (blue), t_{f,h_0}^* (blue dashed), $t_{p,d}^*$ (cyan), and t_{p,h_0}^* (cyan dashed) are shown (colour figure online)



varying levels of N was discussed previously, the relatively large particle sizes used has allowed all cases of Q to be surface tension independent at all scales. Figure 11a shows that $(Bo/Ca)^\alpha$ decreases as Bo/Ca increases for all cases of $Fr_{x,L}$. Given that column collapses are gravity-driven processes, the rate at which gravitational forces increase will dominate the rate at which inertial forces increase for all phases and scales. This means that column mobility, and therefore $t_{x,L}^*$, increases as gravitational force contributions increase with respect to viscous effects.

Figure 11b demonstrates that $(\rho^*)^\beta$ increases with ρ^* in all cases. According to Bougouin and Lacaze [9], the range of ρ_p/ρ_f values used categorises the observed flow states into the inertial regime where inertial fluid forces have a significant impact on flow behaviour. However, the influence of particle inertia still dominates, which causes β to vary depending on the phase of the flow. Generally, the magnitude of β is greater for the particle phase for both quantities of interest at both the column- and granular-scales. It would be interesting to achieve higher values of ρ^* by either reducing ρ_f or increasing ρ_p and see how flow states where fluid inertial effects are no longer important (i.e. the free-fall regime) scale with Eq. 4.

Warnett et al. [8] found that increasing r^* increased the mobility of the collapse in the dry case. In the current study, Fig. 11c shows that the influence of r^* is predominantly dependent on the scale of interest. Generally, increasing r^* reduced the mobility of the column at the column-scale while increasing it at the grain-scale with respect to velocity and collapse duration. This outcome is logical as r^* is a ratio between the column- and grain-scales. Previously, this effect was found to saturate when $r^* \approx 107$, a value that is significantly higher than what is covered by the parameter space of the current study. As r^* was varied by changing the particle size, we are unable to determine whether r_0 , and other parameters defining the column geometry, have a significant impact on the evolution of the flow as N increases.

7 Discussion

The wide particle size distribution in debris flows coupled with comparatively high fluid volume fraction leads to macro-scale flow features that can originate from micro-scale processes. This makes similitude between laboratory experiments and geophysical-scale movement events particularly difficult. For example, surface tension can not be important in the geophysical flow when considering overall flow scale, but becomes important in a laboratory prototype with reduced geometric scale. This means that the true role of surface tension through fines in the geophysical flow may actually be masked by these scaling artefacts in the

laboratory. This research attempts to evaluate laboratory flows where the particles are inertial, in an attempt to isolate the response of those grains as differentiated from fine grains in a debris flow.

To mimic debris flows, we used a just-saturated granular column collapse configuration, consisting of glass grains in a size range where their inertia was significant, facilitated by using a geotechnical centrifuge. Grain size, gravitational acceleration and fluid viscosity were systematically varied to analyse their influence on the front evolution of grain and fluid phases alongside the basal pore pressure.

The drainage phase, where the fluid front accelerates away from the granular front, was found to be accentuated by both increasing the granular pore space and, increasing the level of gravitational acceleration up until $N = 14$. Larger tested values of N resulted in collapse dynamics becoming less dependent on grain-fluid interactions and particle inertia dominating the dynamics of the granular phase. Without enhanced gravitational acceleration, just-saturated granular columns evolved in a similar way to previous experiments (dry, underwater, saturated); comprising acceleration, quasi-steady and retardation phases. The duration of these run out events primarily decreased with particle size as larger capillary forces, which limit grain mobility, developed within the granular materials with smaller pore spaces. In contrast, the collapse duration of tests exposed to elevated levels of gravitational acceleration decreased with both increasing pore space and increasing N for a given particle size. The latter showing that the influence of capillary forces on the evolution of the collapse reduces with increased scale.

Analysis of the temporal evolution of the basal pore pressure at the centre of the column also highlighted the major influence of pore space as N increases, particularly during the initial drainage phase post-collapse initiation. The magnitude of the initial pressure drop increases with decreasing particle size at a given level of elevated gravitational acceleration. Similarly to the conclusions of previous authors [13, 46], this pore size dependent pressure drop is surmised to emanate from the pore-pressure feedback loop for a dense granular configuration. The presence of capillary forces within the just-saturated column configuration caused the pore pressure to drop further when the particle size was smaller.

Buckingham's Π theorem was used to postulate a relationship between 11 fundamental test variables that characterise the acceleration phase of each column collapse using 8 independent dimensionless Π groups. A non-linear regression scheme was used to evaluate the influence of each parameter and found that all measured quantities of interest, specifically, \dot{P}_m^* , $Fr_{x,L}$ and $t_{x,L}^*$, are independent of each other at all scales and are well described by $Q = (Bo/Ca)^\alpha (\rho^*)^\beta (r^*)^\gamma$ where α , β and γ are dependent on Q . Crucially, the inclusion

of both Bo and Ca within a single parameter means that all quantities of interest are decoupled from grain-scale surface tension effects and it is the balance of column-scale gravitational and viscous forces that govern acceleration phase collapse behaviour as seen in natural-scale debris flows with a granular phase including inertial particles.

The current study has been effective in highlighting the collapse response of grain-fluid mixtures with inertial grains. This provides a start point for exploring separately the role of fines, where their effect may be negligible on the inertial/flow scale, but which may nevertheless control processes within the much smaller pore spaces. This work is timely given the findings of Kaitna et al. [15] highlighting the importance of fine granular material to the maintenance of excess pore pressures in steady-state granular-fluid flows. Developing a large dataset of unsteady granular-fluid flow experiments, where the impact of including fine granular material can be quantified, will be crucial to the development of a more mechanically precise pore pressure evolution model.

Acknowledgements The authors would like to acknowledge the contributions of Sam Cook and Steve Lawton for assisting with the development and operation of the experimental apparatus, and Chris Johnson for many useful discussions.

Funding Funding provided by the EPSRC through the doctoral training grant EP/T517902/1.

Declarations

Conflict of interest The authors declare that they have no conflict of interest.

Supplementary content The raw video files for all completed tests are available at <https://doi.org/10.17639/nott.7277>.

Open Access This article is licensed under a Creative Commons Attribution 4.0 International License, which permits use, sharing, adaptation, distribution and reproduction in any medium or format, as long as you give appropriate credit to the original author(s) and the source, provide a link to the Creative Commons licence, and indicate if changes were made. The images or other third party material in this article are included in the article's Creative Commons licence, unless indicated otherwise in a credit line to the material. If material is not included in the article's Creative Commons licence and your intended use is not permitted by statutory regulation or exceeds the permitted use, you will need to obtain permission directly from the copyright holder. To view a copy of this licence, visit <http://creativecommons.org/licenses/by/4.0/>.

References

- Iverson, R.M.: The physics of debris flows. *Rev. Geophys.* **35**(3), 245–296 (1997). <https://doi.org/10.1029/97RG00426>
- Kessler, M., Heller, V., Turnbull, B.: A laboratory-numerical approach for modelling scale effects in dry granular slides. *Landslides* **15**(11), 2145–2159 (2018). <https://doi.org/10.1007/s10346-018-1023-z>
- Forterre, Y., Pouliquen, O.: Flows of dense granular media. *Annu. Rev. Fluid Mech.* **40**(1), 1–24 (2008). <https://doi.org/10.1146/annurev.fluid.40.1.11406.102142>
- Iverson, R.M., Logan, M., LaHusen, R.G., Berti, M.: The perfect debris flow? aggregated results from 28 large-scale experiments. *J. Geophys. Res.* **115**(F3), 03005 (2010). <https://doi.org/10.1029/2009JF001514>
- Lube, G., Huppert, H.E., Sparks, R.S.J., Hallworth, M.A.: Axisymmetric collapses of granular columns. *J. Fluid Mech.* **508**, 175–199 (2004). <https://doi.org/10.1017/S0022112004009036>
- Lajeunesse, E., Mangeney-Castelnau, A., Vilotte, J.P.: Spreading of a granular mass on a horizontal plane. *Phys. Fluids* **16**(7), 2371–2381 (2004). <https://doi.org/10.1063/1.1736611>
- Lajeunesse, E., Monnier, J.B., Homsy, G.M.: Granular slumping on a horizontal surface. *Phys. Fluids* **17**(10), 103302 (2005)
- Warnett, J., Denissenko, P., Thomas, P., Kiraci, E., Williams, M.: Scalings of axisymmetric granular column collapse. *Granul. Matter* **16**(1), 115–124 (2014). <https://doi.org/10.1007/s10035-013-0469-x>
- Bougouin, A., Lacaze, L.: Granular collapse in a fluid: different flow regimes for an initially dense-packing. *Phys. Rev. Fluids* **3**(6), 064305 (2018). <https://doi.org/10.1103/PhysRevFluids.3.064305>
- Artoni, R., Santomaso, A.C., Gabrieli, F., Tono, D., Cola, S.: Collapse of quasi-two-dimensional wet granular columns. *Phys. Rev. E* **87**(3), 032205 (2013). <https://doi.org/10.1103/PhysRevE.87.032205>
- Iverson, R.M.: Scaling and design of landslide and debris-flow experiments. *Geomorphology* **244**, 12 (2015)
- Bougouin, A., Lacaze, L., Bonometti, T.: Collapse of a liquid-saturated granular column on a horizontal plane. *Phys. Rev. Fluids* **4**(12), 124306 (2019). <https://doi.org/10.1103/PhysRevFluids.4.124306>
- Rondon, L., Pouliquen, O., Aussillous, P.: Granular collapse in a fluid: role of the initial volume fraction. *Phys. Fluids* **23**(7), 073301 (2011). <https://doi.org/10.1063/1.3594200>
- McArdell, B.W., Bartelt, P., Kowalski, J.: Field observations of basal forces and fluid pore pressure in a debris flow. *Geophys. Res. Lett.* (2007). <https://doi.org/10.1029/2006GL029183>
- Kaitna, R., Palucis, M.C., Yohannes, B., Hill, K.M., Dietrich, W.E.: Effects of coarse grain size distribution and fine particle content on pore fluid pressure and shear behavior in experimental debris flows. *J. Geophys. Res. Earth Surf.* **121**(2), 415–441 (2016). <https://doi.org/10.1002/2015JF003725>
- Kowalski, J., McElwaine, J.N.: Shallow two-component gravity-driven flows with vertical variation. *J. Fluid Mech.* **714**, 434–462 (2013)
- Iverson, R.M., George, D.L.: A depth-averaged debris-flow model that includes the effects of evolving dilatancy. i. physical basis. *Proc. R. Soc. A Math. Phys. Eng. Sci.* **470**(2170), 20130819 (2014). <https://doi.org/10.1098/rspa.2013.0819>
- Bouchut, F., Fernández-Nieto, E.D., Koné, E.H., Mangeney, A., Narbona-Reina, G.: A two-phase solid-fluid model for dense granular flows including dilatancy effects: comparison with submarine granular collapse experiments. *EPJ Web Conf.* **140**, 09039 (2017). <https://doi.org/10.1051/epjconf/201714009039>
- Taylor, R.N.: *Geotechnical Centrifuge Technology*. Blackie Academic & Professional, New York (1995)
- Milne, F.D., Brown, M.J., Knappett, J.A., Davies, M.C.R.: Centrifuge modelling of hillslope debris flow initiation. *CATENA* **92**, 162–171 (2012). <https://doi.org/10.1016/j.catena.2011.12.001>
- Vallejo, L., Estrada, N., Taboada, A., Caicedo, B., Silva, J.: Numerical and physical modeling of granular flow. In: *Physical Modelling in Geotechnics. Proceedings of the Sixth International Conference on Physical Modelling in Geotechnics*, 6th ICPMG, vol. 6 (2006)

22. Brucks, A., Arndt, T., Ottino, J.M., Lueptow, R.M.: Behavior of flowing granular materials under variable g . *Phys. Rev. E* **75**(3), 032301 (2007)
23. Bowman, E., Take, W., Rait, K., Hann, C.: Physical models of rock avalanche spreading behaviour with dynamic fragmentation. *Can. Geotech. J.* **49**(4), 460–476 (2012)
24. Ng, C.W.W., Choi, C.E., Koo, R., Goodwin, S., Song, D., Kwan, J.S.: Dry granular flow interaction with dual-barrier systems. *Géotechnique* **68**(5), 386–399 (2018)
25. Zhang, B., Huang, Y.: Impact behavior of superspeed granular flow: insights from centrifuge modeling and dem simulation. *Eng. Geol.* **299**, 106569 (2022)
26. Bowman, E.T., Laue, J., Imre, B., Springman, S.M.: Experimental modelling of debris flow behaviour using a geotechnical centrifuge. *Can. Geotech. J.* **47**(7), 742–762 (2010). <https://doi.org/10.1139/T09-141>
27. Buckingham, E.: On physically similar systems; illustrations of the use of dimensional equations. *Phys. Rev.* **4**(4), 345 (1914)
28. Lide, D.R.: *CRC Handbook of Chemistry and Physics*, vol. 85. CRC Press, Boca Raton (2004)
29. Takamura, K., Fischer, H., Morrow, N.R.: Physical properties of aqueous glycerol solutions. *J. Petrol. Sci. Eng.* **98–99**, 50–60 (2012). <https://doi.org/10.1016/j.petrol.2012.09.003>
30. Ellis, E., Cox, C., Yu, H., Ainsworth, A., Baker, N.: A new geotechnical centrifuge at the university of nottingham, UK. In: 6th International Conference of Physical Modelling in Geotechnics: ICPMG, vol. 6, pp. 129–133 (2006)
31. Thompson, E.L., Huppert, H.E.: Granular column collapses: further experimental results. *J. Fluid Mech.* **575**, 177–186 (2007). <https://doi.org/10.1017/S0022112006004563>
32. Legros, F.: The mobility of long-runout landslides. *Eng. Geol.* **63**(3–4), 301–331 (2002). [https://doi.org/10.1016/S0013-7952\(01\)00090-4](https://doi.org/10.1016/S0013-7952(01)00090-4)
33. Cabrera, M., Estrada, N.: Granular column collapse: analysis of grain-size effects. *Phys. Rev. E* **99**(1), 012905 (2019). <https://doi.org/10.1103/PhysRevE.99.012905>
34. Dullien, F.A.: *Porous Media: Fluid Transport and Pore Structure*. Academic Press, San Diego (2012)
35. Sarlin, W., Morize, C., Sauret, A., Gondret, P.: Collapse dynamics of dry granular columns: from free-fall to quasistatic flow. *Phys. Rev. E* (2021). <https://doi.org/10.1103/physreve.104.064904>
36. Li, P., Wang, D., Niu, Z.: Unchanneled collapse of wet granular columns in the pendular state: dynamics and morphology scaling. *Phys. Rev. Fluids* (2022). <https://doi.org/10.1103/physrevfluids.7.084302>
37. Scaramuzza, D., Siegwart, R.: A new method and toolbox for easily calibrating omnidirectional cameras. In: *International Conference on Computer Vision Systems: Proceedings* (2007)
38. Blaber, J., Adair, B., Antoniou, A.: Ncorr: open-source 2d digital image correlation matlab software. *Exp. Mech.* **55**(6), 1105–1122 (2015). <https://doi.org/10.1007/s11340-015-0009-1>
39. Matlab: Version 9.8.0.1451342 (R2020a) The MathWorks Inc., Natick, Massachusetts (2020)
40. Cabrera, M., Mathews, J., Wu, W.: Granular flows in the centrifuge. In: *Proceedings of the 3rd European Conference on Physical Modelling in Geotechnics (EUROFUGE 2016)* (2016)
41. Cabrera, M., Leonardi, A.: On the scaling principles of kinematic processes in a centrifugal acceleration field. In: *Proceedings of the 10th International Conference on Physical Modelling in Geotechnics* (2022)
42. Blajan, M., Umeda, A., Shimizu, K.: Surface treatment of glass by microplasma. *IEEE Trans. Ind. Appl.* **49**(2), 714–720 (2013). <https://doi.org/10.1109/TIA.2013.2244543>
43. Cabrera, M.A., Leonardi, A., Peng, C.: Granular flow simulation in a centrifugal acceleration field. *Géotechnique* **70**(10), 894–905 (2020). <https://doi.org/10.1680/jgeot.18.P.260>
44. Leonardi, A., Cabrera, M.A., Pirulli, M.: Coriolis-induced instabilities in centrifuge modeling of granular flow. *Granul. Matter* **23**(2), 52 (2021). <https://doi.org/10.1007/s10035-021-01111-8>
45. Major, J.J., Iverson, R.M.: Debris-flow deposition: effects of pore-fluid pressure and friction concentrated at flow margins. *Geol. Soc. Am. Bull.* **111**(10), 1424–1434 (1999)
46. Iverson, R.M., Reid, M.E., Iverson, N.R., LaHusen, R.G., Logan, M., Mann, J.E., Brien, D.L.: Acute sensitivity of landslide rates to initial soil porosity. *Science* **290**(5491), 513–516 (2000). <https://doi.org/10.1126/science.290.5491.513>

Publisher's Note Springer Nature remains neutral with regard to jurisdictional claims in published maps and institutional affiliations.